Preclinical Safety of RNAi-Mediated HTT Suppression in the Rhesus Macaque as a Potential Therapy for Huntington's Disease

Jodi L McBride[1,2], Mark R Pitzer[1,*], Ryan L Boudreau[3], Brett Dufour[1], Theodore Hobbs[4], Sergio R Ojeda[1] and Beverly L Davidson[3,5–7]

[1]Division of Neuroscience, Oregon National Primate Research Center, Beaverton, Oregon, USA; [2]Department of Neurology, Oregon Health and Science University, Portland, Oregon, USA; [3]Department of Internal Medicine, University of Iowa, Iowa City, Iowa, USA; [4]Division of Animal Resources, Oregon National Primate Research Center, University of Iowa, Iowa City, Iowa, USA; [5]Department of Neurology, University of Iowa, Iowa City, Iowa, USA; [6]Department of Molecular Physiology, University of Iowa, Iowa City, Iowa, USA; [7]Department of Biophysics, University of Iowa, Iowa City, Iowa, USA
[*]Current address: Department of Social and Behavioral Sciences, University of Portland, Portland, Oregon, USA

To date, a therapy for Huntington's disease (HD), a genetic, neurodegenerative disorder, remains elusive. HD is characterized by cell loss in the basal ganglia, with particular damage to the putamen, an area of the brain responsible for initiating and refining motor movements. Consequently, patients exhibit a hyperkinetic movement disorder. RNA interference (RNAi) offers therapeutic potential for this disorder by reducing the expression of *HTT*, the disease-causing gene. We have previously demonstrated that partial suppression of both wild-type and mutant *HTT* in the striatum prevents behavioral and neuropathological abnormalities in rodent models of HD. However, given the role of *HTT* in various cellular processes, it remains unknown whether a partial suppression of both alleles will be safe in mammals whose neurophysiology, basal ganglia anatomy, and behavioral repertoire more closely resembles that of a human. Here, we investigate whether a partial reduction of *HTT* in the normal non-human primate putamen is safe. We demonstrate that a 45% reduction of rhesus *HTT* expression in the mid- and caudal putamen does not induce motor deficits, neuronal degeneration, astrogliosis, or an immune response. Together, these data suggest that partial suppression of wild-type *HTT* expression is well tolerated in the primate putamen and further supports RNAi as a therapy for HD.

Received 14 September 2011; accepted 14 September 2011; published online 25 October 2011. doi:10.1038/mt.2011.219

INTRODUCTION

Huntington's disease (HD) is a fatal, dominantly inherited, neurodegenerative disorder caused by an expanded trinucleotide (CAG) mutation in the *HTT* gene on chromosome 4.[1] The encoded protein, mutant huntingtin (mHTT), contains an expanded polyglutamine stretch at the N-terminus, conferring a toxic gain of function. Over time, mHTT induces the formation of inclusions, cellular dysfunction, and neurodegeneration throughout the basal ganglia and overlaying cortex. Cell loss in HD is accompanied with upregulation of reactive astrocytes (astrogliosis) and activation of microglia, the resident immune cells of the brain.[2] Although cell loss is observed in multiple brain regions, neuropathology is most pronounced in the medium-sized spiny neurons of the putamen and the caudate, regions of the brain which are critical for the initiation and refinement of motor programs, procedural learning, and various aspects of cognitive function.[3–5] Accordingly, HD patients are afflicted with involuntary hyperkinetic movements of the torso, arms, legs, and face (known as chorea) with concomitant gait and coordination difficulties, working memory deficits, and a variety of emotional disturbances.[6]

To date, HD remains incurable. While several therapies have shown promise in rodent models of the disease, including glutamate antagonists,[7,8] bioenergetic supplements,[9] caspase inhibitors,[10] antihistaminergic agents (HORIZON trial) and fetal tissue transplantation,[11] none have made a significant impact on disease prevention or extension of life span when evaluated in clinical trials. As a result, current treatment strategies are primarily aimed at palliative care to treat disease symptoms and improve end-stage quality of life measures. With the elucidation of the causative HD mutation in 1993,[1] therapies can now be tailored toward reducing expression of the deleterious gene itself, which may have a higher clinical impact compared to strategies aimed at targeting downstream consequences of mHTT.

Recently, it has become clear that endogenous, small microRNAs (miRNAs) play a vital role in regulating the expression of genes during development, throughout adulthood and can contribute to disease states.[12] Endogenous miRNA machinery can be co-opted and used to suppress genes of interest. Exogenous expression of engineered miRNAs as triggers for RNA interference (RNAi) confers a robust decrease in gene expression and

Correspondence: *Jodi L McBride, Division of Neuroscience, Oregon National Primate Research Center and Department of Neurology, Oregon Health and Science University, 505 NW 185th Avenue, Beaverton, OR 97006, USA. E-mail: mcbridej@ohsu.edu or, Beverly L Davidson, Departments of Internal Medicine, Neurology, Molecular Physiology & Biophysics, 200 Eckstein Medical Research Building, University of Iowa, Iowa City, IA 52242, USA. E-mail: beverly-davidson@uiowa.edu*

has been investigated as a therapeutic tool to silence expression of disease alleles.[13] Inarguably, the preferred mechanism to treat HD would be to specifically target the mutant allele while leaving the normal allele intact. As a proof-of-principle, the benefit of allele-specific silencing has been demonstrated by our laboratory members and others in rodent models of HD, wherein inhibitory RNAs were designed to silence the human m*HTT* transgene and not endogenous mouse *Htt*.[14–16] Additionally, several single nucleotide polymorphisms (SNPs) that differentiate up to 80% of diseased and normal alleles have been identified in the human population.[17] However, the utility of these SNPs for RNAi-based silencing strategies have not been tested *in vivo* and importantly, will be unusable for a significant number of HD patients.

Thus, an alternative strategy is to partially reduce expression of both the mutant and normal allele in regions of the brain most affected by the disease, a therapy that would be applicable to all HD patients. Because normal HTT has been found to play a functional role in the adult brain, with proposed roles in mediating transcription[18] and axonal transport,[19] nonallele-specific RNAi treatment for HD must demonstrate therapeutic benefit of reducing the mutant allele, as well as the safety and tolerability of partially suppressing the normal allele. Over the past half-decade, we have used recombinant adeno-associated viral vectors (rAAV) to deliver RNAi silencing constructs to the striatum and showed that a 60% reduction of human *mHTT* and endogenous wild-type mouse *Htt* was well tolerated and prevented motor and neuropathological deficits in transgenic mouse models of HD.[20,21] Additionally, lentiviral delivery of inhibitory RNAs in a rat model of HD conferred a 35% knockdown of *Htt* gene expression (both mutant and wild-type alleles) and was safe and beneficial (both neuroanatomical and behavioral benefits) out to 9 months after injection.[22] Furthermore, heterozygous *Htt* knockout mice are phenotypically normal,[23] and humans with only one copy of *HTT* (50% reduction of normal *HTT* production) show no abnormal behavioral deficits, suggesting that nonallele-specific reduction of HTT expression may be safe.

While findings from rodent models are encouraging, it is essential to evaluate the safety of partial *HTT* suppression in an animal that more closely resembles humans with regards to the size, anatomy, and neurophysiology of its basal ganglia as well as its behavioral capabilities prior to RNAi evaluation in human HD patients. Therefore, in this study, we assessed the safety of reduced *HTT* expression in the rhesus macaque putamen. We demonstrate a partial, sustained *HTT* reduction in the putamen without the development of abnormal motor phenotypes, altered circadian behavior, fine motor skill deficits, neuronal loss, gliosis, or an immune response, thus bringing RNAi closer to the clinic as a potential therapy for HD.

RESULTS

AAV2/1 distribution and *HTT* suppression in the putamen

A sequence that silences mouse, rhesus, and human *HTT* and a control sequence were cloned into an artificial miRNA backbone based on miR-30 and subsequently cloned into AAV, serotype 1, vectors.[24] Expression of the HD-specific miRNA (miHDS1) and the control miRNA (miCONT) was driven by a mouse U6 promoter (**Figure 1a**). Enhanced GFP (eGFP) was driven from a cytomegalovirus (CMV) promoter to allow for assessment of vector distribution following injection into the putamen (**Figure 1b**). Both miHDS1 (targeting a sequence in exon 52 of rhesus HTT mRNA) and miCONT (a control miRNA) were designed using "safe seed" guidelines to optimize safety and minimize potential off-target gene silencing.

Prior to *in vivo* assessment in the rhesus macaque putamen, we first verified *HTT* mRNA suppression by *in vitro* transfection of AAV shuttle plasmids expressing miHDS1, miCONT, or eGFP in human HEK293 cells as well as rhesus primary fibroblasts generated at the Oregon National Primate Research Center (50% and 32% reduction of relative HTT/18S mRNA expression, respectively). Additionally, 60% silencing of striatal Htt mRNA expression, without toxicity, was verified 4 weeks following injection of AAV2/1-miHDS1 injections into both wild-type and BACHD transgenic mice (data not shown).

Following verification of effective *HTT* mRNA suppression *in vitro* and in mice, eleven rhesus macaques received bilateral, MRI-guided stereotaxic injections of either AAV2/1-miHDS1-eGFP (therapeutic miRNA, $n = 4$), AAV2/1-miCONT-eGFP (control miRNA, $n = 4$) or AAV-eGFP (viral vector control, $n = 3$) into

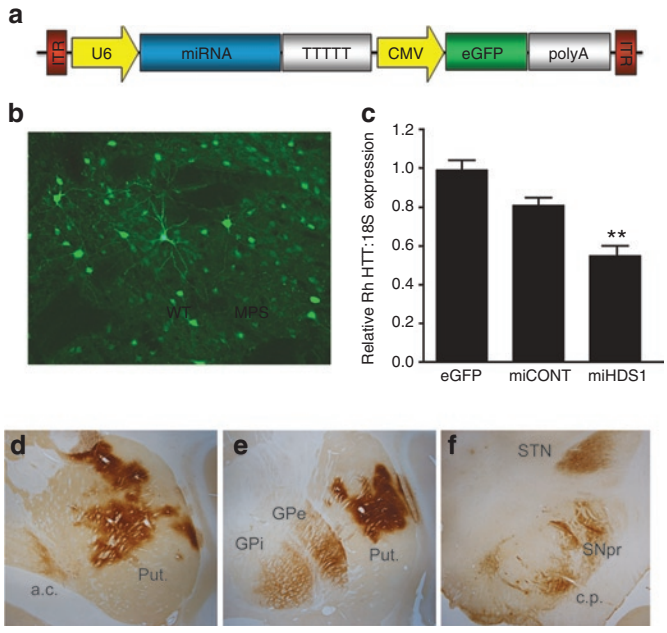

Figure 1 HTT suppression and AAV distribution following injection into the putamen. (**a**) Cartoon of the AAV2/1 vector depicting miRNA expression driven from the Pol III promoter, U6, and eGFP driven from the Pol II promoter, CMV. (**b**) Unstained, eGFP fluorescence was used to define AAV2/1 transduced regions of the putamen. (**c**) Relative rhesus HTT/18S expression was determined by QPCR. AAV-miHDS1-injected putamen showed a significant 45% reduction in HTT expression compared to AAV-eGFP-injected controls (mean ± SEM, $P < 0.01$). Anti-eGFP immunohistochemistry was used to identify (**d**) transduced regions of the putamen and (**e**) other basal ganglia nuclei such as the internal and external segments of the globus pallidus, (**f**) the substantia nigra pars reticulata and the subthalamic nucleus. a.c., anterior commissure; c.p., cerebral peduncle; GPe, exterior segment of the globus pallidus; GPi, interior segment of the globus pallidus; Put., putamen; QPCR, quantitative polymerase chain reaction; SNpr, substantia nigra pars reticulata; STN, subthlamic nucleus.

the commissural and postcommissural putamen (posterior half of the entire putamen). Animals were assessed prior to and for six weeks postsurgery on a variety of general behavior and motor skill assays and euthanized for molecular (tissue punches taken from the left hemisphere) and histological analyses (immuno-stained sections through the right hemisphere). Putamen samples transduced with AAV2/1 (2 × 4 mm) were obtained from the left hemisphere of unfixed, coronal brain slabs at necropsy. Quantitative polymerase chain reaction (QPCR) using primers flanking the miHDS1 targeting site in exon 52 demonstrated a significant reduction of rhesus HTT mRNA transcripts (45%, $P < 0.01$) following injection with AAV1-miHDS1 compared to AAV-eGFP control-treated putamen (**Figure 1c**). We have previously demonstrated, in separate experiments, that similar levels of silencing of either mutant human or wild-type Htt transcripts in mouse striatum cause marked reductions in the respective proteins.[20,21] eGFP immunohistochemistry was conducted to assess viral vector distribution throughout the basal ganglia. eGFP-positive cells were observed throughout the mid- and posterior putamen, indicating accurate needle placements during surgery (**Figure 1d**). Immunofluorescence staining, using eGFP fluorescence as a reference, demonstrated AAV2/1 transduction in dopamine- and cAMP-regulated neuronal phosphoprotein (DARPP-32)-positive medium spiny projection neurons (**Supplementary Figure S1a–c**), choline acetyl transferase (ChAT)-positive large, cholinergic interneurons (**Supplementary Figure S1d–f**), and glial fibrillary acid protein (GFAP)-positive astrocytes (**Supplementary Figure S1g–i**) throughout the putamen. eGFP-positive cells did not co-localize with IBA-1-stained microglia (**Supplementary Figure S1j–l**). In addition to eGFP-positive neurons, astrocytes and fibers observed in the putamen, eGFP-positive cell bodies, and fibers were also seen in other regions of the basal ganglia which receive projections from and project to the putamen. These include the internal and external segments of the globus pallidus (**Figure 1e**), the subthalamic nucleus (fibers only, **Figure 1f**), and the substantia nigra pars reticulata (**Figure 1f**). eGFP expression in the cortex was limited to the needle tracts, suggesting that AAV2/1 was not transported anterogradily and retrogradily to the cortex, as was observed in other regions.

Unbiased stereology was employed to quantify the area fraction of putamen containing eGFP-positive cells and fibers using serial sections stained with anti-eGFP antibody. Results demonstrated an area fraction of eGFP-positive cells in the commissural and postcommissural putamen of 30 ± 2.0% for AAV-eGFP-injected animals, 29 ± 3.0% for AAV-miCONT-injected animals, and 30 ± 3.0% for AAV-miHDS1 animals with no significant differences between groups ($P > 0.05$, **Figure 2a**). Additionally, quantification of the estimated volume of putamen containing eGFP-postive cells and fibers was performed. The mean estimated volume of transduced putamen was 1.0e11 ± 1.7e10 μm^3 for AAV-GFP-injected animals, 8.5e10 ± 5.6e9 μm^3 for AAV-miCONT-injected animals, and 9.9e10 ± 1.6e10 μm^3 for AAV-miHDS1 animals. No significant difference in volume was found between treatment groups (**Figure 2b**, $P > 0.05$). A three-dimensional model of AAV2/1-transduced putamen (right hemisphere only) was created for each animal using Stereo Investigator software, and a representative model from an AAV-HDS1-injected animal is shown in **Figure 2c** with area of the putamen that constitutes eGFP-positive cells depicted in green and the commissural and postcommissural putamen depicted in purple. The 3D rendering allows for the visualization of the three injection sites as well as the spread of vector following surgery. The anterior–posterior (A–P) distribution of eGFP-positive cells, a one-dimensional measure of AAV2/1 distribution from rostral to caudal, was determined from one hemisphere of each of the eleven AAV2/1-injected animals. The mean A–P distribution for transduced putamen was 10.0 ± 1.0 mm for AAV-GFP-injected animals, 9.5e10 ± 1.0 mm for AAV-miCONT animals, and 9.5 ± 0.58 mm for AAV-miHDS1 animals with no significant differences in spread between groups (**Table 1**, $P > 0.05$).

HTT suppression does not induce motor skill deficits

To assess whether partial *HTT* suppression in the putamen, a region of the brain heavily involved in initiating, executing, and refining motor movement, induces motor perturbations, a variety of behavioral assays were used to evaluate the monkeys prior to and for six weeks following surgery. We chose behavioral assays that allowed for the detection of changes in whole body movements in the homecage over 24-hour spans, more specific coordinated movements of the arms and legs and learned tasks requiring higher levels of dexterity of the forearms and digits.

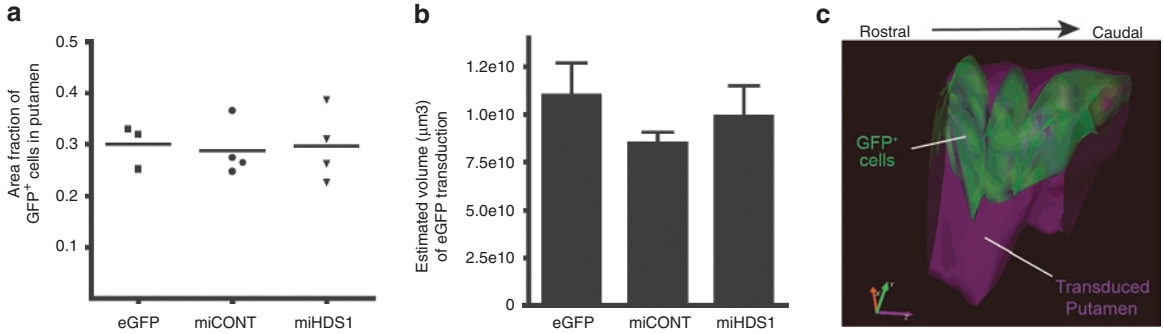

Figure 2 Area fraction and volume of eGFP expression in the putamen. Unbiased stereology was used to determine the (**a**) area fraction and (**b**) volume (μm^3) of eGFP-positive cells in the putamen. No differences in area fraction or volume of eGFP transduction was seen between groups ($P > 0.05$ for both analyses). (**c**) A three-dimensional model was created from volumetric data to demonstrate the distribution of eGFP-positive cells (shown in green) in the targeted putamen (commissural and postcommissural putamen, shown in purple).

Table 1 Measurement of anterior–posterior spread of eGFP-positive regions of the putamen in individual animals injected with AAV2/1-eGFP (n = 3), AAV-miHDS1 (n = 4), or AAV2/1-miCONT (n = 4)

Animal ID	Group	AP spread (mm)
Rh24522	AAV2/1-eGFP	10.0
Rh24906	AAV2/1-eGFP	9.0
Rh25433	AAV2/1-eGFP	11.0
Mean ± SD		10 ± 1.0
Rh24277	AAV2/1-miHDS1	10.0
Rh24353	AAV2/1-miHDS1	9.0
Rh24530	AAV2/1-miHDS1	9.0
Rh25300	AAV2/1-miHDS1	10.0
Mean ± SD		9.5 ± 0.58
Rh24377	AAV2/1-miCONT	9.0
Rh25150	AAV2/1-miCONT	11.0
Rh25388	AAV2/1-miCONT	9.0
Rh25416	AAV2/1-miCONT	9.0
Mean ± SD		9.5 ± 1.0

No differences in AP spread between groups of animals were detected ($P > 0.05$).

To collect daytime and nighttime homecage activity, animals were fitted with nylon or aluminum collars that housed an enclosed Actical accelerometer. All monkeys wore activity collars for 3 weeks prior to surgery. The Actical monitor contains an omnidirectional sensor that integrates the speed and distance of acceleration and produces an electrical current that varies in magnitude depending on a change in acceleration. The monitors were programmed to store the total number of activity counts during each 1-minute epoch. For daytime activity, a repeated measures ANOVA failed to detect significant differences between treatment groups, F (2,64) = 0.17, P = 0.84, suggesting that a partial reduction of HTT in the commissural and postcommissural putamen does not alter general homecage activity levels compared to controls (**Figure 3a**). A significant effect was indicated for time, F (8, 64) = 2.4, $P < 0.05$, and Holms–Sidak pairwise comparisons showed that daytime activity during the week immediately following surgery (+1) was significantly less than the activity exhibited during week −2 ($P < 0.001$) or week +5 ($P < 0.001$), likely owing to a small decrease in overall daytime activity while animals recovered from surgery. No group differences were observed ($P = 0.45$). Likewise, for night time homecage activity, a repeated measures ANOVA indicated no significant differences between treatment groups F (2,64) = 0.189, P = 0.83, nor over time F (8,64) = 1.43, $P = 0.20$ (**Supplementary Figure S2**). Similarly, no interaction was indicated (P = 0.64). In addition to overall circadian homecage activity, body weight from each animal was recorded at surgery and at necropsy, and no decrease in weight was detected in any animal ($P > 0.05$, **Figure 3b**).

Potential changes in fine motor skills of left and right forelimbs and digits were assessed using the Lifesaver test of manual dexterity originally described by Bachevalier *et al.*[25] and further modified by Gash and colleagues.[26] Animals were transported from their homecage to a Wisconsin General Testing Apparatus in a separate behavioral room and trained to remove hard, round treats from a straight medal rod (straight post, **Figure 3d**). For the straight post, animals were assessed 2 weeks prior to surgery to collect baseline data and weekly for 6 weeks after surgery (two trials per forelimb each day, twice a week). No statistical difference was detected in the latencies to remove stimuli from posts between the right and left hands. Consequently, the right and left hand data were collapsed, and averages were used for all analyses. A repeated measures, two-way ANOVA indicated a significant main effect of time over the testing trials, F (6, 48) = 27.5, $P < 0.0001$, indicating that animals from all treatment groups removed the treat from the post with shorter latencies (faster performance) as the study progressed. By contrast, no significant effects were found between the treatment groups, F (2,48) = 0.07, P = 0.99, nor for an interaction (P = 0.55), indicating that AAV-miHDS1-treated animals performed with the same speeds as animals from both control groups (**Figure 3c**). For the Lifesaver task using the question mark shaped post (**Figure 3e**), animals received no training prior to surgery so that we could assess each animal's ability to learn a new and more difficult task (procedural learning) following AAV-miHDS1 injection into the putamen. Beginning 2 weeks following surgery and each week thereafter, latencies to successfully remove each treat off the question mark shaped post were recorded (two trials per forelimb each day, twice a week). A repeated measures two-way ANOVA failed to indicate significant differences between groups, F (2,28) = 0.573, P = 0.58, or over testing trials, F (4,28) = 0.61, P = 0.652 nor for an interaction (P = 0.93). These data show that animals from all treatment groups were able to complete the question mark post task with equal speed and that *HTT* suppression did not alter the ability of the AAV-HDS1-treated animals to (1) learn a new behavioral task or (2) exhibit fine motor skills on a difficult task compared to controls (**Figure 3f,g**) (**Supplementary Videos S1–S4**).

Additionally, we developed a non-human primate-specific, preclinical motor rating scale (MRS) that was modified from the Unified Huntington's Disease Rating Scale used for evaluating motor performance in HD patients. We designed the MRS to specifically assess putamen-based behavioral phenotypes in monkeys including horizontal and vertical ocular pursuit, treat retrieval with both forelimbs, ability to bear weight on both hindlimbs, posture, balance, and startle response. In addition, the scale includes negative motor phenotypes seen in HD or cases of putamen dysfunction including bradykinesia (slowness of movement), dystonia (involuntary, sustained muscle contraction), and chorea (involuntary, hyperkinetic movement) of each limb and trunk (**Supplementary Table S1**). Possible scores ranged from 0 (normal phenotype) to 3 (severely abnormal phenotype) for a total of 72 possible points. Animals were rated by three, independent observers blind to treatment group and familiar with non-human primate behavioral repertoires; inter-rater reliability was 100%. All animals were evaluated in their homecage and were rated once prior to surgery and each week thereafter for the duration of the study. Kruskal–Wallis statistical analysis revealed a significant difference between the three treatment groups (H(2) = 9.30, P = 0.010). However, this difference is due to one AAV-miCONT-injected animal that exhibited a very mild but progressive dystonia in one hind leg (animal 25150). A Dunn's pairwise comparison shows no difference between AAV-miHDS1-injected animals compared to AAV-eGFP-injected controls, demonstrating that a partial *HTT* suppression in the mid- and posterior putamen

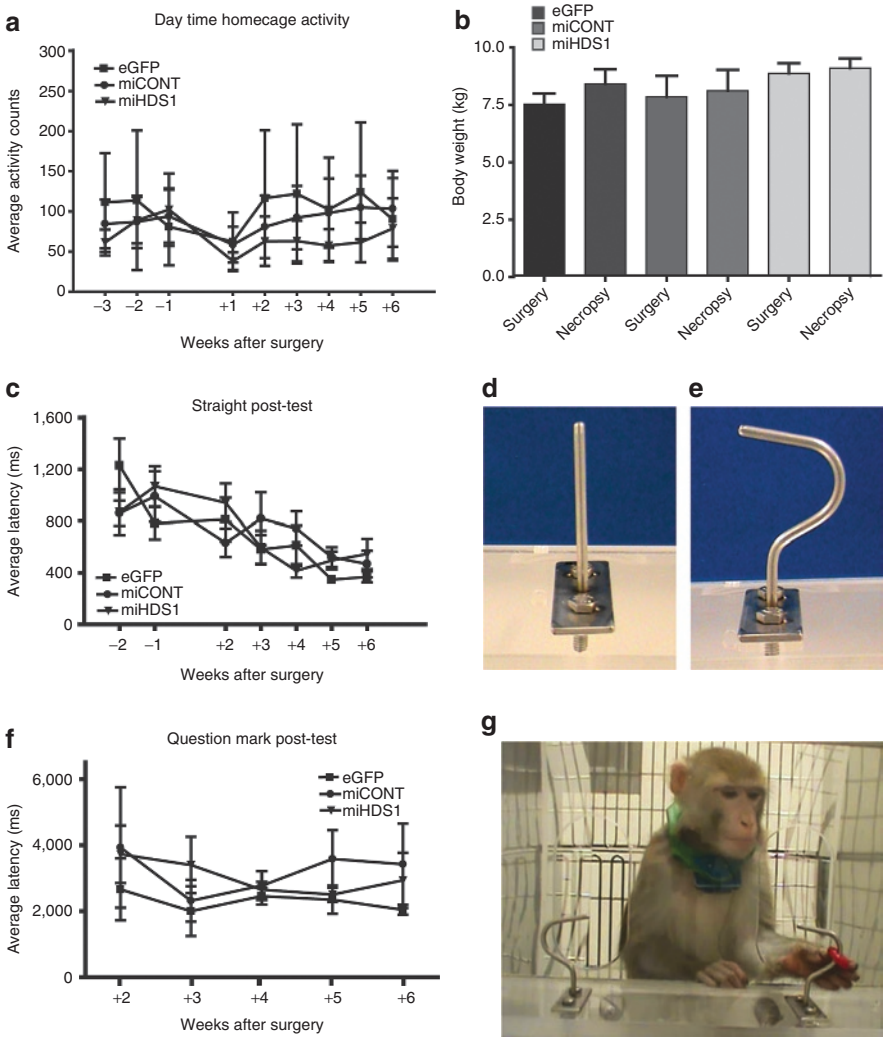

Figure 3 Behavioral analysis of HTT suppression in the putamen. (**a**) Average counts of homecage, daytime activity were assessed using activity monitors mounted onto collars worn by each animal. No significant differences were detected between groups over time ($P > 0.05$, repeated measures ANOVA using animal group and time as variables). (**b**) Body weights taken immediately prior to surgery and at the time of necropsy were not significantly different between groups ($P > 0.05$). (**c**) Time course of average latencies to remove treats from (**d**) a straight metal post indicate no significant differences in performance between the treatment groups ($P > 0.05$) although all groups significantly increased their speed in removing the treat over the duration of the study ($P < 0.001$). (**f**) Average latencies to remove treats from (**e**,**g**) a question mark–shaped metal rod indicate no significant differences in performance between groups ($P > 0.05$). $n = 4$ animals per group for AAV-miHDS1- and AAV-miCONT-injected animals; $n = 3$ for AAV-eGFP-injected animals.

did not alter normal putamen-based behavior nor induce diseased phenotypes commonly seen with neuronal dysfunction or degeneration in the putamen.[27,28]

HTT suppression does not cause neuronal degeneration, gliosis, or inflammation

To address whether *HTT* reduction in cells of the putamen caused neuronal degeneration, we evaluated potential neurotoxicity by immunohistochemical staining for eGFP (**Figure 4a–d**) to identify transduced regions of the putamen, NeuN (neuronal marker), GFAP (astroctyic marker), and Iba1 (microglial marker). Coronal brain sections were stained using standard DAB immunohistochemistry, and adjacent sections were compared for signs of neuron loss, increases in astrocyte proliferation (reactive astrocyosis) or increases in reactive microglia in AAV-miHDS1-treated monkeys compared to controls. Compared to AAV-eGFP- and AAV-miCONT-injected controls, AAV-miHDS1-injected animals showed no loss of NeuN-positive neurons in the putamen (**Figure 4e–h**, transduced regions outlined in black, AAV-miCONT-injected sections not shown). Cresyl violet (Nissl) staining of adjacent coronal brain sections further supported a lack of neuronal loss (data not shown). To assess whether partial *HTT* suppression was associated with cellular dysfunction, in contrast to frank neuronal loss, we performed QPCR analysis for DARPP-32, a highly expressed protein in GABA-ergic projection neurons of the putamen. DARPP-32 is a key mediator in numerous signal transduction cascades, and its downregulation has been reported in cases of medium spiny neuronal dysfunction in the absence of NeuN downregulation.[29] Consequently, DARPP-32 is a valid and reliable readout of neuronal function in the putamen.

QPCR analysis of transduced regions of the putamen found no significant decrease of DARPP-32 mRNA expression in monkeys injected with AAV-miHDS1 compared to controls (**Figure 4q**, $P > 0.05$).

Coronal stained sections from all treatment groups showed a mild increase in GFAP-positive astrocytes in transduced regions, likely due to the injection itself and not a reduction in HTT since equal astrocytosis was observed in all groups (**Figure 4i–l**). IBA-1-stained sections from animals in each group showed no increases in activated microglia, except for within the injection tracts, likely due to physical perturbation of parenchyma by the needle (**Figure 4m–p**). To further assess inflammation, expression of the pro-inflammatory cytokines interleukin 1-β (IL1-β) and tumor necrosis factor-α (TNF-α) was measured from transduced regions. Both of these cytokines are upregulated and released from astrocytes and microglia in response to distressed, neighboring neurons in the brain. QPCR analysis showed no significant increases in IL1-β (**Figure 4r**, $P > 0.05$) or TNF-α (**Figure 4s**, $P > 0.05$) in AAV-miHDS1-treated monkeys compared to AAV-eGFP control animals. Interestingly, monkeys injected with AAV-

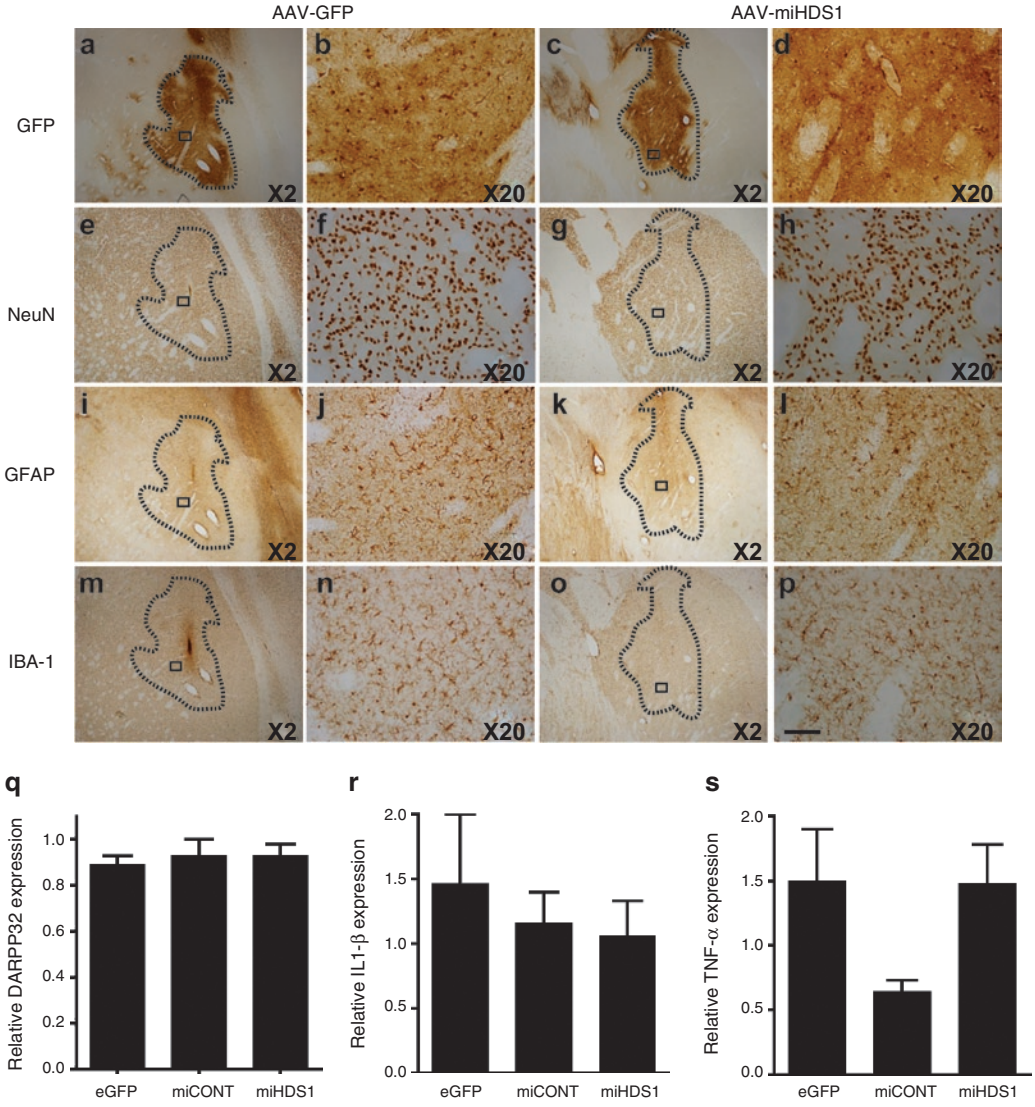

Figure 4 Immunohistochemical and QPCR assessment of neuronal, glial, and inflammatory markers in the putamen. Adjacent, 40-µm-thick sections through the putamen of animals injected with AAV-eGFP ($n = 3$, two left columns), AAV-miHDS1 ($n = 4$, two right columns), or AAV-miCONT ($n = 4$, not shown) were stained with neuronal (NeuN), astrocytic (GFAP), or microglial (IBA-1) markers. Areas outlined with dashed lines in the low magnification (×2) photomicrographs show regions of putamen transduced with eGFP; adjacent sections were matched for landmarks. Small rectangles show the corresponding regions used for high magnification (×20) photomicrographs. (**a–d**) Coronal sections of the putamen in animals from both groups stained for eGFP exhibit intensely stained neurons and astrocytes. Coronal sections of the putamen stained for NeuN show no signs of neuron loss in (**g,h**) AAV-miHDS1-treated monkeys compared to (**e,f**) AAV-eGFP-injected controls. Tissue sections from animals in both (**i,j**) AAV-eGFP and (**k,l**) AAV-miHDS1 groups labeled with GFAP exhibit a slight astrogliosis corresponding to regions of GFP positivity. (**m–p**) Tissue stained with the microglial marker IBA-1 exhibits no qualitative intensity differences between groups in eGFP-positive regions. However, increased immunoreactivity was observed along the needle tract (**m**). Scale bar = 1.0 mm for low and 45 µm for high magnification photomicrographs, respectively. QPCR was used to quantify relative expression levels of (**q**) DARPP-32 and the pro-inflammatory cytokines (**r**) IL1-β and (**s**) TNF-α from tissue punches obtained from AAV2/1-transduced putamen.

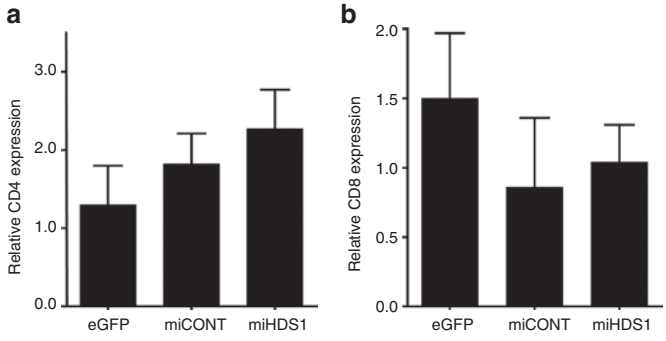

c

Animal ID	Animal ID	6 weeks post surgery
25416	1:160	1:160
25433	1:40	1:80
24277	1:40	1:80
25388	1:10	1:10
25150	N/a	1:40
24530	1:5	1:20
24906	1:5	1:10
24522	<5	<5
24377	<5	<5
25300	<5	<5
24353	<5	<5
Anti-AAV1 rabbit serum control	1:20,480	

Figure 5 Evaluation of a potential peripheral immune response due to HTT silencing or AAV2/1 transduction. QPCR was used to quantify the levels of (**a**) CD4 and (**b**) CD8 mRNA expression in the putamen. No significant difference was observed between groups ($P > 0.05$). **(c)** Neutralizing antibody levels in serum collected prior to surgery and at necropsy from each animal. Neutralizing antibody titers reported are the serum dilutions at which relative luminescence units (RLUs) were reduced by 50% compared to virus control wells. Animals displayed varying levels of neutralizing antibodies prior to and subsequent to surgery. While the majority of injected animals maintained stable antibody levels following surgery, four animals showed slightly higher titers at necropsy (25433, 24277, 24530, and 24906). Fold increase in Nab levels did not correlate with the level GFP transduction in putamen (**Supplementary Figure S2**). $n = 4$ animals per group for AAV-miHDS1- and AAV-miCONT-injected animals, $n = 3$ for AAV-eGFP-injected animals.

miCONT showed a significant decrease in TNF-α expression compared to both AAV-eGFP- ($P < 0.05$) and AAV-miHDS1- ($P < 0.05$) injected animals.

Lack of peripheral immune response following AAV1-miRNA delivery to the putamen

Previous studies have shown that peripheral T cells infiltrate the brain following injury or infection.[30] Thus, in addition to assaying for local inflammatory and immune responses in the putamen, cell-mediated and humoral responses were evaluated to determine whether AAV-mediated suppression of HTT induced peripheral immune responses. Relative CD4 and CD8 mRNA expression levels were determined by QPCR to address whether AAV suppression of *HTT* induced infiltration of peripheral helper or cytotoxic T cells, respectively. No significant differences were seen between groups in either CD4 (**Figure 5a**) or CD8 (**Figure 5b**) mRNA expression in transduced putamen samples ($P > 0.05$). Also, no inflammatory infiltrates were noted on Nissl-stained sections from treated animals (data not shown). To test if anti-AAV antibodies were induced after injection, an *in vitro* neutralizing antibody (Nab) assay was performed on serum collected from each animal immediately prior to surgery and at necropsy (6 weeks after injection). HuH7 cells were infected with AAV2/1 expressing LacZ in the presence of serial dilutions of rhesus serum. The transduction assay showed that the cohort of rhesus macaques used for this study displayed varying levels of neutralizing antibodies to AAV2/1 in their serum prior to surgery ranging from undetectable titers (<1:5) to the highest titer of 1:160 (**Figure 5c**). Four of the 11 animals showed increases in AAV2/1 Nab levels at necropsy but these increases were minor (two- to fourfold). Neither presurgical Nab levels nor the fold change in Nab expression from presurgery to necropsy correlated with levels of eGFP expression in the putamen (Pearson's correlation, $r = -0.24$, $P = 0.49$ and Spearman correlation (**Supplementary Figure S3**; $r = 0.01$, $P = 0.9$, respectively).

DISCUSSION

Here, we present novel data showing that a partial reduction of *HTT* expression in the rhesus macaque putamen is well tolerated out to 6 weeks after injection. We used a multifaceted approach to assess the ability of RNAi to reduce *HTT* and address whether such suppression would induce behavioral or neuropathological consequences by combining assays of gross and fine motor skills with postmortem immunohistochemical, stereological, and molecular analyses of neuronal, glial, and immune profiles. Our silencing construct, miHDS1, was designed such that the target mRNA sequence displays homology to rodent, rhesus macaque, and human *HTT*. Therefore, *HTT* reduction and tolerability can be seamlessly evaluated in transgenic mice and non-human primates. Importantly, the same sequence evaluated preclinically may be utilized to evaluate safety of *HTT* suppression in a phase 1 clinical trial.

The selection of our injection sites in the mid- and posterior putamen was based upon the primate putamen's functional rostral–caudal gradient. Lesions of the posterior aspect of the putamen with excitotoxins[31] or lentiviral-mediated delivery of mutated Htt[28] elicit hyperactivity, choreiform movements, stereotypies, and/or dyskinetic movements of the limbs (either spontaneously or following apomorphine administration). Correspondingly, we have previously observed motor dysfunction detected via the Lifesaver assay and MRS following moderate neuronal loss in the mid- and posterior putamen (unpublished results from our laboratory). By contrast, lesions of the anterior putamen fail to produce similar dyskinesias. These disparate effects correspond with the inputs to the mid- and posterior putamen from the primary sensorimotor cortices including the premotor and supplementary motor areas as well as the primary motor area.[32] By contrast, the anterior primate putamen receives cortical inputs from the frontal association areas, the dorsolateral prefrontal cortices, and the pre-supplementary motor area.[33] Consequently, to assess the tolerability of partial *HTT* suppression in the mid- and posterior putamen, we employed three behavior tests that assess putamen-associated

behaviors. First, to assess potential changes in general activity, we continually assessed homecage activity over the duration of the experiment using omnidirectional activity monitors placed in collars on the animals. No differences in daytime or nighttime activity were found between groups.

In an effort to detect more subtle abnormalities of limb use, muscle tone, eye movements, posture or balance, we devised a MRS based upon the clinical Unified Huntington Disease Motor Rating Scale. Our rubric assessed 24 discrete behaviors and revealed that 10 of the 11 animals showed no behavior anomalies. One AAV-miCONT-injected control animal (no. 25150) displayed a mild dystonia in his left leg. The increased muscle tone in the leg was noted on day 12 subsequent to surgery and may be the result of trauma, infection from the surgical procedure or a perturbation in the putamen due to the injection itself.

To challenge the functional integrity of the mid- and posterior putamen and its circuits, all animals were trained to perform the Lifesaver task. The task requires the animals to rapidly perform a sequence of muscle movements in the arm, hand, and fingers to obtain a reinforcer. For the straight post task, animals were trained for 21 days prior to the initiation of the experiment in an effort to increase animals' efficiency, skill, and speed of performance. Evidence suggests that over-learned sequential hand movements require the functional integrity of the posterior sensorimotor putamen in monkeys[34] and in humans.[35] Consistent with homecage activity and motor ratings, there were no differences in the performance of the straight post task between the HDS1 animals and the controls, again supporting the notion that knockdown of normal *HTT* in the mid- and posterior putamen does not significantly diminish the functional integrity of its circuits.

In contrast to the posterior regions, the anterior and mid-levels of the putamen are known to play an essential role in learning new hand movement sequences.[36] Whereas our intraputamen injections did not cover the entire anterior putamen, eGFP transfection was observed in sections ~3 mm rostral to the anterior commissure. Thus, to assess the potential disruption of a procedural learning circuit, we presented a novel question mark–shaped post 2 weeks following surgery. Despite never being trained on the distinctively shaped post, all groups successfully learned to perform the task at equal rates, suggesting that the relevant putamen circuits were functionally intact. Thus, consistent with homecage activity and motor rating data, partial knockdown of endogenous *HTT* in the mid- and posterior putamen did not diminish the execution of a previously learned motor task nor impair the acquisition of novel manual dexterity task.

We observed robust eGFP expression in both neurons and astrocytes throughout the commissural and postcommissural putamen following injection of each construct. Here, AAV2/1 transduced both DARPP-32-positive medium spiny projection neurons and ChAT-positive large, aspiny interneurons. While medium spiny neurons show the most dramatic cell loss in HD, the large cholinergic neurons are also affected by mHTT. Cholinergic interneurons exhibit decreased levels of ChAT and decreased levels of acetylcholine release in transgenic mouse models of HD as well as HD patients.[37] In contrast to the findings presented here, and by other groups[38] using eGFP as a reporter gene, primarily astrocytic transduction was seen following injection of AAV2/1 expressing humanized renilla GFP (hrGFP) into the cynomolgus macaque putamen.[39] Additionally, a robust anti-hrGFP antibody response was also observed, along with $CD4^+$ lymphocyte infiltration and local microglial responses, suggesting that hrGFP may be less well tolerated in the non-human primate putamen compared to eGFP.

Our finding that AAV2/1 transduces astrocytes, as well as neurons, in the putamen may provide additional benefit in animal models of the disease and in HD patients. While most therapeutic strategies for HD have targeted vulnerable neurons, a growing body of evidence has demonstrated that astrocytes also contain mHTT-positive inclusion bodies. Astrocytes expressing mHTT contain fewer glutamate transporters and are less capable of protecting against glutamate-mediated excitotoxicity. Additionally, Bradford and colleagues demonstrated that double transgenic HD mouse models expressing truncated mHTT in both neurons and glia exhibit more severe neurological symptoms than mice expressing mHtt in neurons alone.[40] Thus, partially suppressing *HTT* in both neurons and glia may have a more robust clinical impact.

eGFP-positive neurons and fibers, but not glia, were also found in the internal and external globus pallidus as well as the substantia nigra pars reticulata, indicating retrograde and anterograde transport of the vector, respectively. eGFP-positive fibers only were seen in the subthalamic nucleus. These findings may have important clinical implications for HD as these regions of the basal ganglia also undergo mHTT-induced cell loss and gliosis. Injections into a single brain region (putamen) may have the capability of therapeutically targeting multiple vulnerable brain regions. Specifically, transduced neurons in the globus pallidus and substantia nigra should also express *HTT*-specific miRNAs and may therefore be amenable to RNAi therapy. Ongoing analyses in our laboratory are currently investigating the levels of miRNA expression and concomitant levels of *HTT* mRNA suppression in these brain regions.

Our immunohistochemical and molecular results demonstrate a significant 45% decrease in HTT, a level of suppression which has shown therapeutic benefit in mouse models of HD without inducing toxicity (targeting both mutant and wild-type alleles). This level of suppression did not induce NeuN-positive cell loss nor downregulate DARPP-32 expression. We detected a very mild upregulation of GFAP-positive astrocytes in transduced regions of the putamen. Because astrogliosis was detected in animals from all three groups, it was not due to a reduction in Htt expression in neighboring neurons. Rather, the mild astrogliosis was likely due to the injection itself. Because brains were evaluated at 6 weeks after injection, this low level of gliosis would be predicted to decrease over time. Importantly, we saw no upregulation in reactive microglia or pro-inflammatory cytokine expression which would be predicted to increase if *HTT* reduction induced neural toxicity.

Recombinant AAV gene transfer to the intact CNS has been shown to elicit a minimal T cell-mediated response without a salient plasma cell-mediated immune response in preclinical animals studies. Additionally, encouraging findings from recent early-stage gene therapy clinical trials for Canavan's Disease (CD),[41] Parkinson's Disease (PD),[42] and Leber's congenital amaurosis (LCA)[43] wherein AAV, serotype 2, was directly injected into

the brain parenchyma (CD, PD) or the retina (LCA), demonstrated only mild increases in Nab levels after injection with no signs of inflammation or adverse neurological events. The results here further support these findings and demonstrate that although monkeys had a range of preexisting, circulating Nab levels prior to surgery (from undetectable up to 1:160), there was no major increase in Nab levels (two- to fourfold maximum) 6 weeks after injection. Moreover, despite the minor increase in Nab levels in 4/11 animals, there was no correlation of Nab levels with the area fraction of GFP^+ cells in the putamen. Interestingly, the presence of preexisting Nab titers at the upper range of what we report has been shown to substantially abrogate gene expression following systemic, intravascular injection of varying serotypes of AAV to target either brain[44] or peripheral tissues.[45] Our data are encouraging and suggest that even though NHPs and humans have natural circulating antibodies to AAV2/1,[46] as well as other serotypes, a preexisting antibody load, at least up to the values reported here, will not limit gene transfer and should not be an exclusion criteria for clinical trials involving direct brain injections.

In summary, our results in the rhesus macaque brain further support and extend previous experiments in rodents demonstrating the safety and efficacy of a nonallele-specific *HTT* reduction. These findings, along with the well-established safety profile of rAAV in early phase clinical trials for a variety of neurological disorders, underscore the potential of viral-mediated RNAi as a therapy for HD.

MATERIALS AND METHODS

Animals. Eleven normal adult rhesus macaques of Indian origin (male, 7–10 kg) were utilized in this study. All monkeys were maintained one per cage on a 12-hour on/12-hour off lighting schedule with ad libitum access to food and water. All experimental procedures were performed according to Oregon National Primate Research Center and Oregon Health and Science University Institutional Animal Care and Use Committee and Institutional Biosafety Committee approved protocols.

RNAi constructs and viral vector production. All siRNAs were generated using an algorithm developed to reduce the off-targeting potential of the antisense sequences.[47] siRNA sequences targeting either a sequence in exon 52 of mouse, rhesus, and human huntingtin or a control siRNA were embedded into an artificial miRNA scaffold comparable to human miR-30 to generate miHDS1 (pri: 5′-AGUGAGCGA UGCUGGCUC GCAUGGUCGAUA CUGUAAAGCCAC AGAUGGGU**GUCGACCA UGCGAGCCAGCAC**CGCCUACU-3′, predicted antisense sequence in bold) or miCONT(pri: 5′-AGUGAGCGCAGCGAAC GACUUACGCGUUU AC UGUAAAGCCACAGAUGGG**UAAACGCGUAA GUCGUUCGCUA** CGC CUACU, predicted antisense sequence in bold). Artificial miRNA stem loops were cloned into a mouse U6 expression vector, and the expression cassettes were subsequently cloned into pFBGR-derived plasmids which coexpress CMV-driven GFP. Shuttle plasmids (pAAVmiHDS1-GFP and pAAVmiCONT-GFP) contain the respective transcriptional units which are flanked at each end by AAV serotype 2 145-bp inverted terminal repeat sequences. rAAV production was performed using the Baculovirus AAV System.[48] Sf9 insect cells were infected with a baculovirus expressing AAV rep2, AAV cap 1, and adenovirus helper proteins and a second baculovirus expressing the miRNA and eGFP flanked by the AAV2 ITR's. The cell lysate was run through an iodixanol gradient (15%–60% wt/vol), and the iodixanol fraction containing the rAAV particles was further purified using a Mustang-Q ion exchange filter membrane. rAAV particle titer was determined by QPCR and FACS analysis. Vectors were generated by the Gene Transfer Vector Core at the University of Iowa and sent to the Oregon National Primate Research Center for injections. Twelve hours before surgery, all viral vector preps were dialyzed against Formulation Buffer 18 (Hyclone) to remove salts (3 total hours of dialysis) and diluted to a final titer of 1e12 vg/ml.

Magnetic resonance imaging and stereotaxic surgery. Immediately prior to surgery, animals were anesthetized with Ketamine HCL (10 mg/kg), transported to the MRI, intubated and maintained on 1% isoflurane vaporized in oxygen for the duration of the scan. Animals were placed into an MRI-compatible, stereotaxic surgical frame; a T1-weighted magnetic resonance image (MRI) was conducted to obtain surgical coordinates (Siemens 3.0 T Trio MR unit). After scanning, animals were taken directly into the operating room and prepped for sterile surgery. Each animal received three microinjections per hemisphere (six injections total): the first 1 mm rostral to the anterior commissure (12 µl) and the two remaining injections (12 µl and 10 µl, respectively) spaced 3 and 6 mm caudal to the first injection. Animals were injected with 1e12 vg/ml of either AAV2/1-miHDS1-eGFP ($n = 4$), AAV2/1-miCONT-eGFP ($n = 4$) or AAV2/1-eGFP ($n = 4$) at a rate of 1 µl/minute, and the needle was left in place for an additional 5 minutes to allow the injectate to diffuse from the needle tip. After microinjections were completed, the skull opening was filled with gelfoam and the incision closed.

Behavioral analysis

General homecage activity: All animals were fitted with either nylon or aluminum collars (Primate Products) with Actical accelerometers (Respironics) mounted onto the frame. Each Actical monitor contained an omnidirectional sensor that integrated the speed and distance of whole body acceleration and produced an electrical current that varies in magnitude depending on a change in acceleration. The monitor was programmed to store the total number of activity counts for each 1-minute epoch. Animals wore activity collars 24 hours a day, 7 days a week for 3 weeks prior to surgery and each week thereafter for the duration of the study.

MRS: Three independent observes, blinded to group identity, assessed homecage behavior weekly. Twenty-four separate putamen-associated behaviors were rated including horizontal and vertical ocular pursuit, treat retrieval with both forelimbs, ability to bear weight on both hindlimbs, posture, balance, startle response and bradykinesias, dystonias and choreas of each limb and trunk. A score of 0 indicated a normal phenotype while a score of 3 indicated severely abnormal phenotypic movements. All animals were evaluated on the MRS prior to surgery to obtain baseline scores and once per week for the duration of the study.

Lifesaver test: Animals were trained to thread edible, hard treats from a straight metal rod (straight post) and then tested on their ability to remove treats from the straight post and a question mark–shaped post. All manual dexterity tasks were presented in a Wisconsin general testing apparatus (WGTA) and the latency to successfully retrieve the treat was measured separately for the left and right forelimbs. Animals were trained for 21 days on the straight post. Then, 2 weeks of baseline data were collected on the straight post only. Two weeks following surgery, animals were tested twice per week on both the straight post and the question mark–shaped post. On testing days, each animal was placed into the WGTA and their movements recorded on digital video. Each hand was tested two times with a time limit of 5 seconds for the straight post and 10 seconds for the question mark post to complete the task. The latency to remove each treat was assessed via Sony PMB software with millisecond measuring capability at a later time.

Necropsy and tissue processing. Six weeks after surgery, animals were sedated with Ketamine and then deeply anesthetized with sodium pentobarbital followed by exsanguination. Brains were perfused through the ascending carotid artery with 2 l of 0.9% saline, removed from the skull, placed into an ice-cold, steel brain matrix and blocked into 4-mm-thick slabs in the coronal plane. Tissue punches used for molecular analyses

were obtained from each animal's left hemisphere of the transduced putamen (slabs were placed under the fluorescent scope to verify eGFP-fluorescing regions) and immediately frozen in liquid nitrogen to preserve DNA, RNA, and protein. Slabs were subsequently postfixed in 4% paraformaldehyde for histological analyses.

Quantitative real-time PCR. RNA was isolated from tissue punches taken from eGFP-positive putamen using the Qiagen RNeasy kit, as per the manufacturer's instructions, and reverse transcribed with random primers and Multiscribe reverse transcriptase (Applied Biosystems, Carlsbad, CA). Relative gene expression was assessed via QPCR by using TaqMan primer/probe sets for DARPP-32 (Hs00259967_m1), CD4 (Rh02621720_m1), CD8 (Rh02839719_m1), IL1-β (Rh02621711_m1), or TNF-α (Rh02789784). All values were quantified by using the ΔΔCT method (normalizing to 18S) and calibrated to AAV-GFP-injected putamen. Primers for rhesus HTT mRNA quantification were designed to flank the miHDS1 binding site in Exon 52 using Primer Express (Applied Biosystems):Forward: 5′-CGGGAGCT GTGCTCACGT-3′, Reverse: 5′-CATTTCTACC CGGCGACAAG-3′), and expression was assessed using SYBR Green detection. At the conclusion, dissociation curve (melting curve) analysis was performed to confirm specific amplification.

Immunohistochemical analyses. 40-µm-thick, free-floating coronal brain sections were processed for immunohistochemical visualization of eGFP expression (eGFP, 1:000, Invitrogen), neurons (NeuN, 1:1000, Millipore), reactive astrocytes (GFAP, 1:2000, DAKO), or microglia (Iba1, 1:1,000; WAKO) by using the biotin-labeled antibody procedure. Following endogenous peroxidase inhibition and washes, tissues were blocked for 1 hour in 5% donkey serum, and primary antibody incubations were carried out for 24 hours at room temperature. Sections were incubated in donkey anti-rabbit or anti-mouse biotinylated IgG secondary antibodies (1:200; Vector Laboratories, Burlingame, CA) for 1 h at room temperature. In all staining procedures, deletion of the primary antibody served as a control. Sections were mounted onto gelatin-coated slides and coverslipped with Cytoseal 60 (Thermo Scientific, Waltham, MA). Images were captured by using an Olympus BX51 light microscope and DP72 digital color camera, along with an Olympus DP Controller software.

Immunofluorescence analyses. 40-µm-thick, free-floating coronal brain sections were processed for immunofluorescent visualization of medium spiny projection neurons (DARPP-32, 1:25, Cell Signaling, Danvers, MA), large cholinergic neurons (ChAT, 1:500, Millipore, Billerica, MA), reactive astrocytes (GFAP, 1:1000, DAKO, Carpinteria, CA), or microglia (Iba1, 1:500; WAKO, Richmond, VA). Following washes, tissues were blocked for 1 hour in 5% donkey serum, and primary antibody incubations were carried out for 24 hours at room temperature. Sections were incubated in donkey anti-rabbit or anti-goat Alexa-546 conjugated secondary antibodies (1:500; Invitrogen, Carlsbad, CA) for 1 hour at room temperature. Sections were mounted onto gelatin-coated slides and coverslipped with Slowfade Gold anti-fade mounting media containing DAPI (Invitrogen). Images were captured at ×20 magnification using a Leica SP5 confocal microscope.

Stereological determination of vector distribution. The Area Fraction Fractionator (Microbrightfield) was used to quantify the fraction of eGFP-positive cells in the putamen (right hemisphere only). Every 12th coronal section (1/2 series, 40-µm-thick sections) through the putamen containing GFP^+ cells was selected for analysis. The putamen was outlined under ×2 magnification, and a rectangular lattice of points was overlaid. One marker was used to select points that fell within the region of interest (putamen), and a second marker was used to select points that fell within the subregion of interest (contained GFP-positive cells). The counting frame area was 1000 × 1000 µm, XY placement was 1600 × 1600 µm, and grid spacing was 120 µm. The area fraction estimation of GFP^+ cells in the putamen was determined by dividing the area of GFP^+ cells by the area of the putamen and estimates provided were averaged from all sections quantified. A 3D reconstruction of the eGFP-transduced putamen was created using StereoInvestigator software by aligning contours from each section from the rostral to caudal putamen and placing skins over each. The anterior to posterior spread of eGFP transduction was determined by locating the most rostral and caudal sections through the putamen containing GFP and using a combined MRI and histology atlas of the rhesus monkey brain (Saleem and Logothetis) to identify the distance between the two (1 mm resolution).

Neutralizing antibody assay. Whole blood was collected in red top Vacutainer Serum Tubes (BD) from animals prior to surgery and at necropsy, serum was collected following centrifugation at 2500 rpm for 20 minutes and stored at −80 °C until analysis. Serum was sent to the Immunology Core at the University of Pennsylvania for analyzing AAV2/1 antibody levels via an *in vitro* transduction assay. A 96 well plate was seeded with Huh7 cells and infected with AAV2/1-LacZ and serial dilutions of pre- and postsurgery rhesus serum. Values reported are the serum dilution at which relative luminescence units (RLUs) were reduced by 50% compared to virus control wells (no serum sample). The lower limit of detection was a 1/5 dilution, and anti-AAV2/1 rabbit serum was used at a positive control.

Statistical analysis. All statistical analyses were performed by using SigmaStat statistical software (SYSTAT). QPCR analyses for HTT, DARPP-32, CD4, CD8, IL1-β, and TNF-α expression, as well as Area Fraction Fractionator analyses, were performed by using a one-way ANOVA. Upon a significant effect, Bonferroni post hoc analyses were performed to assess for significant differences between individual groups. For homecage activity and Lifesaver test analyses, a two-way, repeated measures ANOVA using group and time as variables was run to determine differences between groups or over time. Post hoc analyses were performed when statistically significant differences were detected. For MRS analyses, a Kruskal–Wallis test was run followed by a Dunn's pairwise comparison to detect differences between groups. Correlational data between the area fraction of GFP in the putamen and presurgical Nab levels were determined using a Pearson's correlation for parametric data. Correlational data between the area fraction of GFP in the putamen and the fold change of Nab titers pre- and postsurgery were determined using a Spearman correlation for nonparametric data. In all cases, $P < 0.05$ was considered significant.

ACKNOWLEDGMENTS

We thank Graham Flory, Vincent Warren, and Christopher Kroenke for their assistance with magnetic resonance imaging as well as Greg Dissen, Theodore Hobbs, and Drew Martin for their surgical expertise. Additionally, we thank Kevin Meuller for his expertise and assistance with transfer-box training. We thank Wendy Price and Lakshman Annamalai for necropsy support, as well as Anda Cornea for confocal microscopy expertise. We thank Maria Scheel at the University of Iowa Gene Transfer Vector core for production of the viral vectors. This research was funded by National Institutes of Health Grants NS-50210 (B.L.D.), DK-54759 (B.L.D.), NS068280-01 (J.L.M. and B.L.D.), NS069798-01 (J.L.M.), and ONPRC Core Grants RR000163 (J.L.M.) and RR000163. Confocal microscopy was supported by RR024585 (AC) and NS061800.

SUPPLEMENTARY MATERIAL

Figure S1. Immunofluorescence demonstrating transduced cell types in the putamen.

Figure S2. Time course of nighttime, homecage activity showing no significant difference between the treatment groups ($P > 0.05$).

Figure S3. Correlational analysis between area of eGFP transduction and fold increase of anti-AAV2/1 neutralizing antibodies in serum.

Table S1. Preclinical motor rating scale to assess NHP putamen-based behaviors: an inventory of the 24 behaviors assessed each week in the animals' homecage.

Video S1. AAV-eGFP injected control monkey (animal 24522) performing the question mark post-test of manual dexterity 2 weeks postsurgery.
Video S2. AAV-eGFP injected control monkey (animal 24522) performing the question mark post-test of manual dexterity 6 weeks postsurgery.
Video S3. AAV-miHDS1 injected control monkey (animal 24530) performing the question mark post-test of manual dexterity 2 weeks postsurgery.
Video S4. AAV-miHDS1 injected control monkey (animal 24522) performing the question mark post-test of manual dexterity 6 weeks postsurgery.

REFERENCES

1. Huntington Disease Collaborative Research Group (1993). A novel gene containing a trinucleotide repeat that is expanded and unstable on Huntington's disease chromosomes. The Huntington's Disease Collaborative Research Group. *Cell* **72**(6): 971–983.
2. Vonsattel, JP, Myers, RH, Stevens, TJ, Ferrante, RJ, Bird, ED and Richardson, EP Jr (1985). Neuropathological classification of Huntington's disease. *J Neuropathol Exp Neurol* **44**: 559–577.
3. DeLong, MR, Alexander, GE, Georgopoulos, AP, Crutcher, MD, Mitchell, SJ and Richardson, RT (1984). Role of basal ganglia in limb movements. *Hum Neurobiol* **2**: 235–244.
4. Hedreen, JC and DeLong, MR (1991). Organization of striatopallidal, striatonigral, and nigrostriatal projections in the macaque. *J Comp Neurol* **304**: 569–595.
5. Levy, R, Friedman, HR, Davachi, L and Goldman-Rakic, PS (1997). Differential activation of the caudate nucleus in primates performing spatial and nonspatial working memory tasks. *J Neurosci* **17**: 3870–3882.
6. Jason, GW, Pajurkova, EM, Suchowersky, O, Hewitt, J, Hilbert, C, Reed, J *et al.* (1988). Presymptomatic neuropsychological impairment in Huntington's disease. *Arch Neurol* **45**: 769–773.
7. Schilling, G, Coonfield, ML, Ross, CA and Borchelt, DR (2001). Coenzyme Q10 and remacemide hydrochloride ameliorate motor deficits in a Huntington's disease transgenic mouse model. *Neurosci Lett* **315**: 149–153.
8. Schiefer, J, Landwehrmeyer, GB, Lüesse, HG, Sprünken, A, Puls, C, Milkereit, A *et al.* (2002). Riluzole prolongs survival time and alters nuclear inclusion formation in a transgenic mouse model of Huntington's disease. *Mov Disord* **17**: 748–757.
9. Matthews, RT, Yang, L, Jenkins, BG, Ferrante, RJ, Rosen, BR, Kaddurah-Daouk, R *et al.* (1998). Neuroprotective effects of creatine and cyclocreatine in animal models of Huntington's disease. *J Neurosci* **18**: 156–163.
10. Bantubungi, K, Jacquard, C, Greco, A, Pintor, A, Chtarto, A, Tai, K *et al.* (2005). Minocycline in phenotypic models of Huntington's disease. *Neurobiol Dis* **18**: 206–217.
11. Isacson, O, Dunnett, SB and Björklund, A (1986). Graft-induced behavioral recovery in an animal model of Huntington disease. *Proc Natl Acad Sci USA* **83**: 2728–2732.
12. He, L and Hannon, GJ (2004). MicroRNAs: small RNAs with a big role in gene regulation. *Nat Rev Genet* **5**: 522–531.
13. Davidson, BL and Paulson, HL (2004). Molecular medicine for the brain: silencing of disease genes with RNA interference. *Lancet Neurol* **3**: 145–149.
14. Huang, B, Schiefer, J, Sass, C, Landwehrmeyer, GB, Kosinski, CM and Kochanek, S (2007). High-capacity adenoviral vector-mediated reduction of huntingtin aggregate load *in vitro* and in vivo. *Hum Gene Ther* **18**: 303–311.
15. Franich, NR, Fitzsimons, HL, Fong, DM, Klugmann, M, During, MJ and Young, D (2008). AAV vector-mediated RNAi of mutant huntingtin expression is neuroprotective in a novel genetic rat model of Huntington's disease. *Mol Ther* **16**: 947–956.
16. Harper, SQ, Staber, PD, He, X, Eliason, SL, Martins, IH, Mao, Q *et al.* (2005). RNA interference improves motor and neuropathological abnormalities in a Huntington's disease mouse model. *Proc Natl Acad Sci USA* **102**: 5820–5825.
17. Pfister, EL, Kennington, L, Straubhaar, J, Wagh, S, Liu, W, DiFiglia, M *et al.* (2009). Five siRNAs targeting three SNPs may provide therapy for three-quarters of Huntington's disease patients. *Curr Biol* **19**: 774–778.
18. Zuccato, C, Tartari, M, Crotti, A, Goffredo, D, Valenza, M, Conti, L *et al.* (2003). Huntingtin interacts with REST/NRSF to modulate the transcription of NRSE-controlled neuronal genes. *Nat Genet* **35**: 76–83.
19. Szebenyi, G, Morfini, GA, Babcock, A, Gould, M, Selkoe, K, Stenoien, DL *et al.* (2003). Neuropathogenic forms of huntingtin and androgen receptor inhibit fast axonal transport. *Neuron* **40**: 41–52.
20. McBride, JL, Boudreau, RL, Harper, SQ, Staber, PD, Monteys, AM, Martins, I *et al.* (2008). Artificial miRNAs mitigate shRNA-mediated toxicity in the brain: implications for the therapeutic development of RNAi. *Proc Natl Acad Sci USA* **105**: 5868–5873.
21. Boudreau, RL, McBride, JL, Martins, I, Shen, S, Xing, Y, Carter, BJ *et al.* (2009). Nonallele-specific silencing of mutant and wild-type huntingtin demonstrates therapeutic efficacy in Huntington's disease mice. *Mol Ther* **17**: 1053–1063.
22. Drouet, V, Perrin, V, Hassig, R, Dufour, N, Auregan, G, Alves, S *et al.* (2009). Sustained effects of nonallele-specific Huntingtin silencing. *Ann Neurol* **65**: 276–285.
23. Duyao, MP, Auerbach, AB, Ryan, A, Persichetti, F, Barnes, GT, McNeil, SM *et al.* (1995). Inactivation of the mouse Huntington's disease gene homolog Hdh. *Science* **269**: 407–410.
24. Boudreau, RL, Monteys, AM and Davidson, BL (2008). Minimizing variables among hairpin-based RNAi vectors reveals the potency of shRNAs. *RNA* **14**: 1834–1844.
25. Bachevalier, J, Landis, LS, Walker, LC, Brickson, M, Mishkin, M, Price, DL *et al.* (1991). Aged monkeys exhibit behavioral deficits indicative of widespread cerebral dysfunction. *Neurobiol Aging* **12**: 99–111.
26. Gash, DM, Zhang, Z, Umberger, G, Mahood, K, Smith, M, Smith, C *et al.* (1999). An automated movement assessment panel for upper limb motor functions in rhesus monkeys and humans. *J Neurosci Methods* **89**: 111–117.
27. Burns, LH, Pakzaban, P, Deacon, TW, Brownell, AL, Tatter, SB, Jenkins, BG *et al.* (1995). Selective putaminal excitotoxic lesions in non-human primates model the movement disorder of Huntington disease. *Neuroscience* **64**: 1007–1017.
28. Palfi, S, Brouillet, E, Jarraya, B, Bloch, J, Jan, C, Shin, M *et al.* (2007). Expression of mutated huntingtin fragment in the putamen is sufficient to produce abnormal movement in non-human primates. *Mol Ther* **15**: 1444–1451.
29. Régulier, E, Trottier, Y, Perrin, V, Aebischer, P and Déglon, N (2003). Early and reversible neuropathology induced by tetracycline-regulated lentiviral overexpression of mutant huntingtin in rat striatum. *Hum Mol Genet* **12**: 2827–2836.
30. Jander, S, Lausberg, F and Stoll, G (2001). Differential recruitment of CD8+ macrophages during Wallerian degeneration in the peripheral and central nervous system. *Brain Pathol* **11**: 27–38.
31. Hantraye, P, Riche, D, Maziere, M and Isacson, O (1990). A primate model of Huntington's disease: behavioral and anatomical studies of unilateral excitotoxic lesions of the caudate-putamen in the baboon. *Exp Neurol* **108**: 91–104.
32. Hoover, JE and Strick, PL (1993). Multiple output channels in the basal ganglia. *Science* **259**: 819–821.
33. Selemon, LD and Goldman-Rakic, PS (1985). Longitudinal topography and interdigitation of corticostriatal projections in the rhesus monkey. *J Neurosci* **5**: 776–794.
34. Lehéricy, S, van de Moortele, PF, Lobel, E, Paradis, AL, Vidailhet, M, Frouin, V *et al.* (1998). Somatotopical organization of striatal activation during finger and toe movement: a 3-T functional magnetic resonance imaging study. *Ann Neurol* **44**: 398–404.
35. Maillard, L, Ishii, K, Bushara, K, Waldvogel, D, Schulman, AE and Hallett, M (2000). Mapping the basal ganglia: fMRI evidence for somatotopic representation of face, hand, and foot. *Neurology* **55**: 377–383.
36. Gerardin, E, Pochon, JB, Poline, JB, Tremblay, L, Van de Moortele, PF, Levy, R *et al.* (2004). Distinct striatal regions support movement selection, preparation and execution. *Neuroreport* **15**: 2327–2331.
37. Smith, R, Chung, H, Rundquist, S, Maat-Schieman, ML, Colgan, L, Englund, E *et al.* (2006). Cholinergic neuronal defect without cell loss in Huntington's disease. *Hum Mol Genet* **15**: 3119–3131.
38. Dodiya, HB, Bjorklund, T, Stansell, J 3rd, Mandel, RJ, Kirik, D and Kordower, JH (2010). Differential transduction following basal ganglia administration of distinct pseudotyped AAV capsid serotypes in nonhuman primates. *Mol Ther* **18**: 579–587.
39. Hadaczek, P, Forsayeth, J, Mirek, H, Munson, K, Bringas, J, Pivirotto, P *et al.* (2009). Transduction of nonhuman primate brain with adeno-associated virus serotype 1: vector trafficking and immune response. *Hum Gene Ther* **20**: 225–237.
40. Bradford, J, Shin, JY, Roberts, M, Wang, CE, Sheng, G, Li, S *et al.* (2010). Mutant huntingtin in glial cells exacerbates neurological symptoms of Huntington disease mice. *J Biol Chem* **285**: 10653–10661.
41. McPhee, SW, Janson, CG, Li, C, Samulski, RJ, Camp, AS, Francis, J *et al.* (2006). Immune responses to AAV in a phase I study for Canavan disease. *J Gene Med* **8**: 577–588.
42. Kaplitt, MG, Feigin, A, Tang, C, Fitzsimons, HL, Mattis, P, Lawlor, PA *et al.* (2007). Safety and tolerability of gene therapy with an adeno-associated virus (AAV) borne GAD gene for Parkinson's disease: an open label, phase I trial. *Lancet* **369**: 2097–2105.
43. Simonelli, F, Maguire, AM, Testa, F, Pierce, EA, Mingozzi, F, Bennicelli, JL *et al.* (2010). Gene therapy for Leber's congenital amaurosis is safe and effective through 1.5 years after vector administration. *Mol Ther* **18**: 643–650.
44. Gray, SJ, Matagne, V, Bachaboina, L, Yadav, S, Ojeda, SR and Samulski, RJ (2011). Preclinical Differences of Intravascular AAV9 Delivery to Neurons and Glia: A Comparative Study of Adult Mice and Nonhuman Primates. *Mol Ther* **19**: 1058–1069.
45. Chirmule, N, Xiao, W, Truneh, A, Schnell, MA, Hughes, JV, Zoltick, P *et al.* (2000). Humoral immunity to adeno-associated virus type 2 vectors following administration to murine and nonhuman primate muscle. *J Virol* **74**: 2420–2425.
46. Calcedo, R, Vandenberghe, LH, Gao, G, Lin, J and Wilson, JM (2009). Worldwide epidemiology of neutralizing antibodies to adeno-associated viruses. *J Infect Dis* **199**: 381–390.
47. Boudreau, RL, Spengler, RM and Davidson, BL (2011). Rational design of therapeutic siRNA: minimizing off-targeting potential to improve the safety of RNAi therapy for Huntington's disease. *Mol. Ther.* 185 (epub ahead of print).
48. Smith, RH, Levy, JR and Kotin, RM (2009). A simplified baculovirus-AAV expression vector system coupled with one-step affinity purification yields high-titer rAAV stocks from insect cells. *Mol Ther* **17**: 1888–1896.